Effect of nitrogen doping on TiOxNy thin film formation at reactive high-power pulsed magnetron sputtering

Vitezslav Stranak, Marion Quaas, Robert Bogdanowicz, Hartmut Steffen, Harm Wulff, Zdenek Hubicka, Milan Tichy, Rainer Hippler

▶ **To cite this version:**

Vitezslav Stranak, Marion Quaas, Robert Bogdanowicz, Hartmut Steffen, Harm Wulff, et al.. Effect of nitrogen doping on TiOxNy thin film formation at reactive high-power pulsed magnetron sputtering. Journal of Physics D: Applied Physics, 2010, 43 (28), pp.285203. 10.1088/0022-3727/43/28/285203 . hal-00569651

HAL Id: hal-00569651
https://hal.science/hal-00569651

Submitted on 25 Feb 2011

HAL is a multi-disciplinary open access archive for the deposit and dissemination of scientific research documents, whether they are published or not. The documents may come from teaching and research institutions in France or abroad, or from public or private research centers.

L'archive ouverte pluridisciplinaire **HAL**, est destinée au dépôt et à la diffusion de documents scientifiques de niveau recherche, publiés ou non, émanant des établissements d'enseignement et de recherche français ou étrangers, des laboratoires publics ou privés.

Effect of nitrogen doping on TiO_xN_y thin film formation at reactive high-power pulsed magnetron sputtering.

Vitezslav Stranak [a,b,*], Marion Quaas [a,c], Robert Bogdanowicz [d], Hartmut Steffen [c], Harm Wulff [a], Zdenek Hubicka [b], Milan Tichy [e] and Rainer Hippler [a]

[a] *Institute of Physics, E.M.U. University of Greifswald, Felix-Hausdorff-Str. 6, 17489 Greifswald, Germany*
[b] *Institute of Physics v. v. i., Academy of Science of the Czech Republic, Na Slovance 2, 182 21 Praha 8, Czech Republic*
[c] *Leibniz Institute for Plasma Science and Technology, Felix-Hausdorff-Str. 2, 17489 Greifswald, Germany*
[d] *Gdansk University of Technology, Narutowicza Street 11/12, 80952 Gdansk, Poland*
[e] *Charles University in Prague, Faculty of Mathematics and Physics, V Holešovičkách 2, 180 00 Prague 8, Czech Republic*

Abstract

The paper is focused on a study of formation of TiO_xN_y thin films prepared by pulsed magnetron sputtering of metallic Ti target. Oxygen and nitrogen were delivered into the discharge in the form of reactive gases O_2 and N_2. The films were deposited by high-power impulse magnetron sputtering working with discharge repetition frequency $f = 250$ Hz at low ($p = 0.75$ Pa) and high ($p = 10$ Pa) pressure. The substrates were on floating potential and thermally stabilized at room temperature during deposition process. Post-deposition thermal annealing was not employed. The chemical composition from XPS diagnostic reveals formation of TiO_xN_y structure at low flow rate of oxygen in the discharge gas mixture. This result is confirmed by XRD investigation of N elements incorporation into the Ti-O lattice. Decrease of band-gap to values $E_g \sim 1.6$ eV in TiO_xN_y thin film is attributed to formed Ti-N bonds. The discharge properties were investigated by time-resolved optical emission spectroscopy. Time evolution of particular spectral lines (Ar^+, Ti^+, Ti) is presented together with peak discharge current.

Key words: TiO_xN_y, HIPIMS, time resolved optical emission spectroscopy, thin film diagnostic (XRD, XPS, spectroscopic ellipsometry)
PACS: 52.25.Jm, 52.70.Kz, 52.77.Dq, 52.80.Vp, 61.05.cp., 81.15.Cd, 82.80.Pv

1. Introduction

Titanium oxide is well known as a photocatalytic material since 1970s [1]. Photocatalytic activity together with other interesting features (high adhesion, hardness, refractive index, transparency, high dielectric constant, semiconducting properties) makes TiO_2 a promising coating material. However, photocatalytic efficiency of pure TiO_2 after irradiation by solar spectrum is very low. Because of high energy band-gap of TiO_2 only the UV part of the solar spectra (< 5 % of solar energy) is able to initiate photocatalytic reactions. Hence, the photocatalytic reactions are strongly reduced in locations with limited UV radiation, e.g. in rooms, etc.

The photocatalytic activity of TiO_2 can be improved by doping. Two basic group of dopants can be used: (i) cations of transition metals such as Fe, Ni, Cr, Mn, V, Ag, Au, which can increase absorption of visible spectra but usually suffer from thermal instability [2–6], and (ii) non-metal anion such as N^- [7–10], C^- [11], S^- [12], F^- [13], which shift the band-

* Corresponding author.
Email address: stranv00@physik.uni-greifswald.de (Vitezslav Stranak).

gap towards lower spectral frequencies. Among the doping elements, N was found to be most effective because (i) nitrogen has comparable ionic radius to oxygen and (ii) the p states of N contribute to band-gap narrowing by mixing with O 2p states [9,14].

Various deposition techniques, e.g. pulsed laser deposition (PLD) [15–17], sol-gel methods [18–20], ion-assisted electron beam evaporation [21,22], magnetron sputtering [10,23–34] have been employed to prepare TiO_xN_y thin films. Owing to its numerous advantages, magnetron sputtering deposition is a well established method for coating which has been already extended to the industry. Nevertheless, deposition of crystalline TiO_xN_y by dc magnetron sputtering method is difficult and the process must be usually followed by thermal annealing [10,18,23,25,28] or high discharge current during deposition is applied [25,26]. However, nowadays, there is a growing need to deposit photocatalytic films on plastic, i.e. heat sensitive, materials. Hence, post-deposition thermal annealing excludes conventional dc magnetron sputtering as a method for industrial coating of TiO_xN_y thin films.

Dc magnetron sputtering was successfully combined with reactive gas pulsing process to get crystalline TiO_xN_y without thermal annealing [29–31]. With the same purpose Herman et al. employed dc pulsed dual magnetron working with repetition frequency 100 kHz and duty cycle 50 % [34]. The method of pulsed magnetron sputtering at medium frequencies was developed in [35] and lastly reviewed in [36]. However, an other method of pulsed magnetron sputtering, so-called HIgh Power Impulse Magnetron Sputtering (HiPIMS) [37–41] is a promising coating technique. Because of high power pulse density ($\sim$ kW/cm^2) HiPIMS is suitable for deposition of oxides in particular phases at low (room) temperature as was shown in [42–44]. In spite of this fact HiPIMS technique has not been yet tested for deposition of TiO_xN_y thin films.

The main goal of our investigation is focused on deposition and formation of TiO_xN_y films by HiPIMS at room temperature. The basic properties of thin films (chemical composition, crystallography, optical properties) are discussed together with comprehensive plasma diagnostic by optical emission spectroscopy.

2. Experimental details

2.1. *Thin film deposition*

Thin TiO_xN_y films were prepared by pulsed planar magnetron sputtering operated in HiPIMS conditions. A detailed description of the experimental setup can be found in our previous papers, see [42,45].

The commercial planar magnetron by Gencoa (Gencoa, Liverpool, UK), operated in unbalanced mode, is employed as a sputtering source. The source was equipped by a Ti target 50 mm in diameter. The sputtering source is situated in the lower part of a spherical-shaped stainless-steel UHV chamber. The vacuum chamber is pumped out by turbomolecular pump down to ultimate pressure 10^{-6} Pa. The working pressure is adjusted by a throttle valve installed between the chamber and the pump. The flow rates of working gases are controlled by MKS flow controllers.

The discharge was excited using a combination of dc power supply AE MDX500 (Advanced Energy, Fort Collins, CO) with range down to -620 V designated for continuous regime and a power switch based on charging of large capacitors during idle part of the pulses. The switch was activated by a signal from waveform generator Agilent 33120A (Agilent, Santa Clara, CA). The generator served for triggering of time-resolved measurements as well. A ballast resistor ($R = 2.1\ \Omega$) serving as dummy load without magnetron discharge was inserted in series with the magnetron cathode path. Instant discharge current was calculated from the difference between voltage waveforms, measured by oscilloscope Tektronix TDS1012 (Tektronix, Richardson, TX), directly on the cathode U_c and on serial connection of resistor R and cathode U_{c+R} using Ohm′s law.

Parameters of TiO_xN_y film deposition process are summarized in Table 1. The flow rates for Ar and N_2 were kept constant while the flow rate of O_2 was varied to get different stoichiometry of thin film composition. Mean discharge current was kept constant ($I_m = 400$ mA) for all experiments. The pulse-modulated discharge was operated with frequency $f = 250$ Hz and pulse width $t_a = 150\ \mu$s.

The substrate holder was on floating potential and cooled by circumfluent water during the deposition. The temperature, measured by a thermocouple situated at the substrate holder plate, was stabilized at $\sim$ 40 °C. However, the temperature

Table 1
Overview of experimental conditions during deposition of TiO_xN_y thin film using pulse-modulated discharge.

abbreviation	value	description
p	0.75 and 10 Pa	pressure
F_{Ar}	20 sccm	flow rate of Ar
F_{N2}	10 sccm	flow rate of N_2
F_{O2}	0.2-10 sccm	flow rate of O_2
f	250 Hz	discharge frequency
t_a	150 μs	pulse width
V_m	370-620 V	cathode voltage
I_m	**400 mA**	mean discharge current
I_D	23-55 A	peak discharge current
i_D	0.5-1.2 A/cm^2	peak current density
P_p	0.3- 0.7 kW/cm^2	peak power density

of the substrate surface/growing film is expected higher as studied e.g. in [46]. The time of deposition was 90 minutes. Films were deposited on polished Si(100) wafers. The thickness of the film was roughly about $\sim$ 100 nm (estimated from XR and SE measurements), i.e. deposition rate 1 - 1.5 nm/min. Resputtering effect of the deposited film is completely neglected because of apparent deposition rate. The adhesion of the films on the substrate was very good and no bubbles or grains were observed.

2.2. *Time-resolved plasma diagnostic*

Pulse-modulated discharge was investigated using optical emission spectroscopy. The measurements were performed by Shamrock SR500D spectrometer (focal length 500 mm) equipped with iCCD detector iStar DH740I both by Andor (Andor Technology, Belfast, Northern Ireland). The spectrometer was equipped with three gratings 300, 1200 and 2400 lines per milimeter. The wavelength resolution of the spectrograph ($\sim$ 0.1 nm) is sufficient to allow accurate evaluation of measured data. The optical fibre, connected with the spectrometer, was built directly into the vacuum chamber. The fiber was placed at a distance of 65 mm from the target surface, i.e. in the position of substrate holder. The range of scanned spectra were λ = (200-850) nm. The pulse generator Agilent 33120A provided triggering signal for iCCD. The measured spectra were analyzed by Spectrum Analyzer 1.7 [47].

2.3. *Thin film characterization*

Grazing incidence x-ray diffraction (GIXD, asymmetric Bragg case) measurements were done to determine the phase composition of deposited films, the respective methods are described e.g. in [48]. All measurements were performed using Θ-2Θ-Diffractometer Siemens D5000 (Bruker AXS GmbH, Karlsruhe, Germany) with Cu Kα radiation (40 V, 40 mA). The scanned 2Θ range was 20 to 50° at constant incidence angle ω = 1.0°. The Powder Diffraction File was used to assign the measured x-ray reflections and identify the crystallographic phases [49]. From XR measurements we can conclude that the films are homogeneous because XR data can be very well fitted with a model with assuming constant film density.

The chemical composition of the thin films was investigated by x-ray photoelectron spectroscopy (XPS). The analyses were performed on an AXIS Ultra x-ray photoelectron spectrometer (Kratos Analytical, Manchester, UK) with a monochromatic Al K_α x-ray source at 150 W (15 kV, 10 mA). A survey scan from 0 to 1200 eV was mapped with a pass energy of 80 eV. For high resolution measurements of the Ti 2p peak a pass energy of 10 eV was used. The quantification was done from the measured area of the XPS peaks, considering atomic sensitivity factors (ASF) given by the producer. The program package CasaXPS 2.3.15 was used for characterization. The validity of the ASF was checked by measuring samples of given composition (SiO_2 and TiO_2). Gaussian + Lorentzian functions with relation 30:70 % were employed for fitting the measured data. Shirley background was used for fitting of Ti 2p XPS peaks.

Ellipsometric investigations were carried out using a phase modulated ellipsometer Jobin-Yvon UVISEL (HORIBA Jobin-Yvon Inc, Edison, NJ) in the 1.8 eV - 4.8 eV photon energy range at an angle of 70°, due to Brewster's angle of Si wafer substrate. Angles Δ and Ψ were analyzed using two-layers model based on TiO_xN_y and Si substrate. The optic indices of Si were obtained from the database [50]. The complex dielectric function of TiO_xN_y was composed of Tauc-Lorentz and Cody-Lorentz oscillators [25,26]. Finally, the model was fitted to the experimental data using Levenberg-Marquardt nonlinear least-squares algorithm. The fitting measure mean square error (MSE) was used for verification of ability of the applied model to

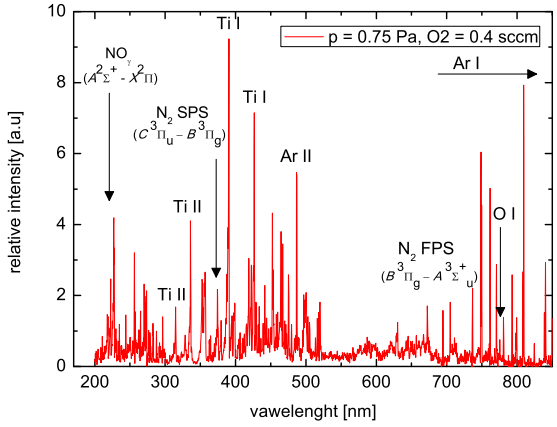

Fig. 1. Overview of the spectrum measured in Ar discharge with O_2 and N_2 reactive admixtures. Experimental conditions: p = 0.75 Pa, F_{Ar} = 20 sccm, F_{N2} = 10 sccm and F_{O2} = 0.4 sccm. The spectrum was recorded at t_a = 50 μs after discharge ignition.

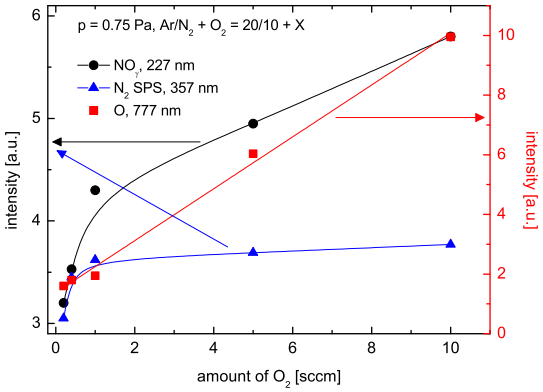

Fig. 2. Plot of intensities of atomic line O and molecular bands of systems N_2 2nd positive and NO_γ vs. amount of O_2 added in the discharge. Experimental conditions: p = 0.75 Pa, F_{Ar} = 20 sccm, F_{N2} = 10 sccm. Intensities were estimated from spectra recorded at t_a = 50 μs after discharge ignition.

fit the experimental data [51]. Band-gap energy E_g was obtained by extrapolating the linear portion to the photon energy in α vs. $E(h\nu)$ graph, where α is the absorption coefficient.

3. Results and discussion

3.1. *Time-resolved diagnostics of plasma discharge*

The overview spectrum of Ar/N_2+O_2 discharge, shown in Fig. 1, mostly consists of the atomic lines of Ar, Ar^+, Ti, Ti^+, O, molecular bands of NO_γ ($A\,^2\Sigma^+ \longrightarrow X\,^2\Pi$) system, which was not observed in the dc-mode, and of the N_2 first and second positive systems ($B\,^3\Pi_g \longrightarrow A\,^3\Sigma^+_u$, $C\,^3\Pi_u \longrightarrow B\,^3\Pi_g$).

We observed strong N_2 bands in the spectrum but only one weak emission series of N (λ_N = 821.1-821.6 nm) was recognized (studied in [52]). Intensity of N lines was roughly three times higher in HiPIMS than in dc mode operated with the same experimental parameters and discharge current. However, we can expect presence of N atoms in the discharge volume as it was already demonstrated in [53]. In the reported experiments the N density, measured by mass spectrometry, reached the order of magnitude 2-4 $\times$ 10^{18} m^{-3} at pressure about 2 Pa. The reactor consists of inductively coupled plasma source fed by argon, nitrogen and sputtered Ti. Hence, we suppose that in our case weak N lines in UV-VIS range of the spectrum are probably overlapped by other intensive lines or disappear in the background of noise.

The spectra and intensities of particular spectral lines are affected by the amount of reactive component O_2 added into the discharge. As expected, the intensity of atomic oxygen line (λ_O = 777 nm) depends nearly linearly on the amount of added O_2, see Fig. 2. The intensity of the N_2 2nd positive system (λ_{N2-SPS} = 357 nm) is observed almost constant for higher O_2 flow rates (F_{O2} = 0.5 -10 sccm). It means that the rate of N_2 excitation in the discharge volume is not significantly effected by oxygen in the plasma. An increase of the NO_γ system (λ_{NO_γ} = 227 nm) was observed with increasing of oxygen partial pressure. It was shown in works [54–56] that NO is preferentially produced as a result of nitrogen and oxygen reaction.

Time evolution of discharge current is shown in Fig. 3. The discharge current was calculated, using Ohm′s law formula, from the voltage drop measured by oscilloscope on the ballast resistor (the method is described in detail in our earlier papers [43,45]). Time evolution of I_D shown in Fig. 3 is typical for low pressure (p = 0.75 Pa) and slightly oxidized gas mixture. Peak discharge current reached about $I_p \approx 23$ A which corresponds to peak power of about $P_p \sim 14.3$ kW.

Discharge current is influenced by partial O_2 pressure. This phenomena can be explained by emission of secondary electrons induced by ion bombardment of oxidized cathode/target; the ion induced secondary electron emission coefficient is

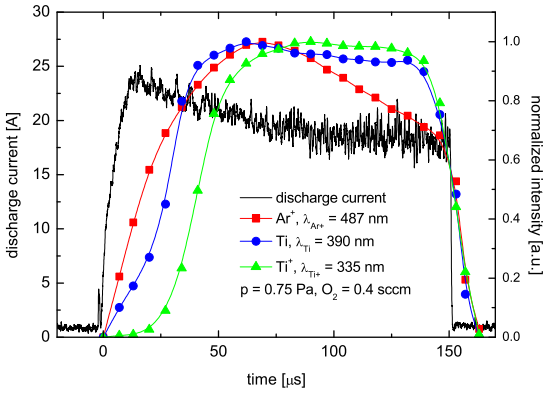

Fig. 3. Time evolution of peak discharge current I_D (black line, left axis) and intensities of atomic spectral lines of Ar^+ (λ_{Ar+} = 487 nm), Ti (λ_{Ti} = 390 nm) and Ti^+ (λ_{Ti+} = 335 nm) during the pulse width (right axis). Experimental conditions: p = 0.75 Pa, F_{Ar} = 20 sccm, F_{N2} = 10 sccm and F_{O2} = 0.4 sccm.

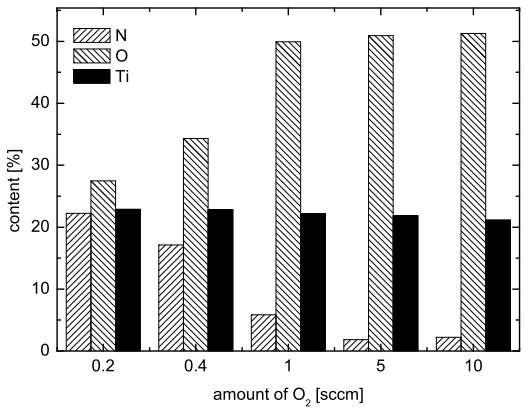

Fig. 4. Chemical composition of TiO_xN_y - Ti, O and N elements are shown. The chemical content is normalized to 100 % - the absent content of elements belongs to impurities (mainly introduced by C) roughly about 25 %. Experimental conditions: p = 0.75 Pa, F_{Ar} = 20 sccm, F_{N2} = 10 sccm.

higher for oxides than for pure metal [42,58]. In this way, at $p = 10$ Pa and highly oxidized gas mixtures, the peak discharge current reaches maximum values $I_D \approx 55$ A (i.e. $P_p \sim 34$ kW) at time $t_a \approx 130$ μs after discharge ignition (not presented in the figure).

Time evolution of peak discharge current and normalized intensities of particular Ar^+ (λ_{Ar+} = 487 nm), Ti (λ_{Ti} = 390 nm) and Ti^+ (λ_{Ti+} = 335 nm) lines is shown in Fig. 3, too. The Ar^+ starts to develop as the first followed by Ti or Ti^+ lines, respectively. Similar features were also observed in a two-component (Ti target, Ar atmosphere) HiPIMS system, where evolution of gas and metallic ions was measured by energy resolving quadrupole spectrometry [59]. Increase of pressure, p =10 Pa, or oxygen flow results in a slower evolution of emitted lines.

The ratio of the measured relative intensities $I_{Ar+}/I_{Ti} \sim 0.6$ is more or less constant in the first half of the pulse width. This effect probably corresponds to re-sputtering of TiN film from the target surface poisoned by nitrogen ($Y_{TiN} = 0.43$ for Ar^+, $Y_{TiN} = 0.37$ for N^+ ion energies of 500 eV [60]). After removal of the nitride film from target surface, the ratio of intensities decreases if the amount of oxygen in the discharge is low: $F_{O2} \lesssim 0.5$ sccm. Such effect is caused by higher sputtering yield of pure metallic target surface ($Y_{Ti} = 0.63$ for Ar^+, $Y_{Ti} = 0.46$ for N^+ for ion energies of 500 eV [60]).

The effect of target poisoning was studied by measurements of hysteresis loops [61–63] and XPS analysis of the target surface after discharge operation. Since the N_2 with higher partial pressure was used for all experiments the target surface can be considered as TiN. When O_2 was added into discharge atmosphere we observed transition of target state mode from -nitride to -oxynitride indicated by an increase of cathode voltage and also verified by measurement of the target surface composition. We observed broader hysteresis loops for poisoning of pure Ti than TiN target surface by oxygen. The poisoning transition was observed for oxygen flow rate F_{O2} = 0.5 - 1.1 sccm. For oxygen flow higher than 1.1 sccm target becomes fully poisoned and intensity of Ti line rapidly decreases, i.e. $I_{Ar+}/I_{Ti} > 1$, due to lower sputtering yield of oxides ($Y_{TiO_x} = 0.015$ for Ar^+ ion energy of 300 eV [64]). After target poisoning the intensities of gas as well as metal atoms/ions became virtually constant (not shown in the figure).

The time development of the intensity of Ti^+ line ($\lambda_{Ti+} = 335$ nm) is shown in Fig. 3, too. The positive Ti^+ ions are created by ionization of sputtered Ti atoms in plasma volume. Owing to lower ionization potential ($E_{Ti} = 6.82$ eV) Ti atoms are preferentially ionized in comparison to Ar ($E_{Ar} = 15.78$ eV). The preferential ionization of titanium can explain the intensity decrease of Ar^+ line while intensities of Ti and Ti^+ remain constant.

3.2. *Chemical composition - XPS measurements*

The nitrogen content of the films was determined by XPS methods. Fig. 4 shows the element composition of samples deposited at constant pressure ($p = 0.75$ Pa) and nitrogen flow ($F_{N2} = 20$ sccm). The flow rate of oxygen was varied. Thin films consist of Ti, N and O elements. Owing to surface contamination also impurities (mainly carbon) are detected. The content of impurities reached roughly 25 % of the total film composition (not included in Fig. 4). The high impurity/carbon concentration is caused by surface contamination during the transfer of the samples to XPS device. However, we can exclude the presence of TiC structure in the film because C 1s peak does not contribute any TiC.

A decrease of nitrogen content is observed for increasing the O to N ratio for particular deposition of thin films at low pressure, see Fig. 4. At higher pressures there is nearly no change in element composition caused by changing the ratio of the reactive gases in the discharge. Obviously, there is a preferred incorporation of oxygen into the growing film. If a sufficient amount of oxygen is present in the discharge volume, nitrogen is virtually not incorporated. With increasing oxygen flow not only the intensity of the N 1s peak, but also the contributions of TiN to the nitrogen 1s spectrum decreases while O 1s increases.

This observation is confirmed by high resolution measurements of the Ti 2p peak. Fig. 5 shows the Ti 2p peak of the film deposited at $p = 0.75$ Pa with $F_{O2} = 0.2$ sccm oxygen flow. We have to assume three possible bindings to fit the measured profile. The 2p Ti peak was fitted using three contributions: 458.5 eV, 457.1 eV and 455.7 eV correspond to Ti(IV) 2p 3/2, Ti(III) 2p 3/2 and Ti(II) 2p 3/2, respectively. The other three functions in the Fig. 5 correspond to 2p 1/2 peak. Unfortunately, TiO and TiN cannot clearly be distinguished, because both bindings contribute to the Ti(II) peak. The formation of TiO_2 can be attributed to surface oxidation on the film top during transport of the sample from the vacuum chamber to the XPS device in air as was already mentioned. With increasing oxygen ratio the amount of Ti(III) and Ti(II) components is decreasing. For oxygen flow $F_{O2} > 1$ sccm (Fig. 5) the Ti 2p region shows only two peaks which belong to Ti(IV) 2p 3/2 and 1/2 peaks. Because of negligible content of N in the film, the peak at Ti(II)/Ti(III) position was not detected. Occasional observation

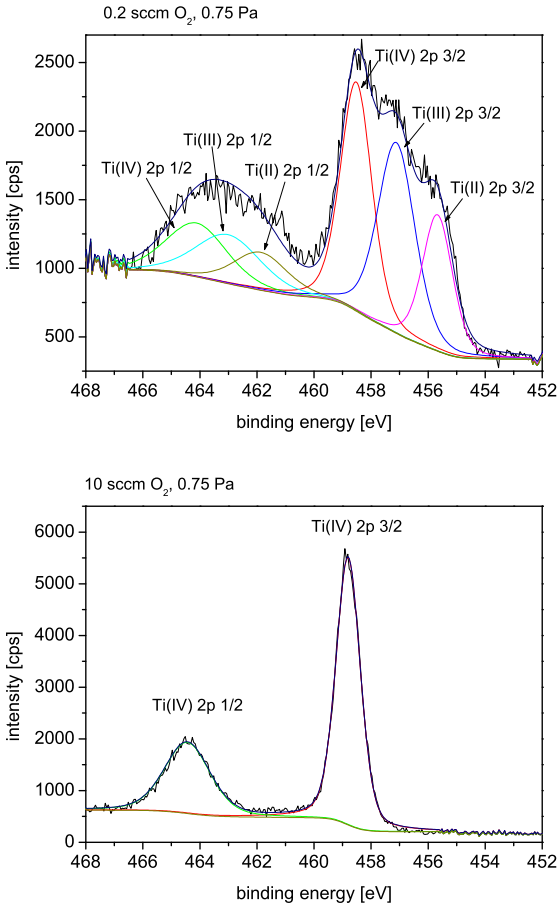

Fig. 5. Ti 2p peaks measured by high resolution XPS measurements of film deposited under pulsed magnetron sputtering conditions: $f = 250$ Hz, $t_a = 150$ μs, $p_c = 0.75$ Pa. Upper graph: The Ti 2p 3/2 peak of film deposited at low oxygen flow $F_{O2} = 0.2$ sccm. The measured data are fitted by three functions Ti(IV), Ti(III) and Ti(II); Lower graph: The Ti 2p 3/2 peak of film deposited at high oxygen flow $F_{O2} = 10$ sccm. The data were fitted only by one function corresponding to Ti(IV).

of weak nitrogen traces is attributed to surface contamination. Hence we can conclude that only TiO_2 is formed for higher oxygen flow rates.

3.3. *Crystallographic phase composition - XRD measurements*

XRD measurements were performed to get information about the phase composition of the layers. As expected from the XPS measurements, TiO/TiN as well as TiO_2 phases are observed (Fig. 6) as a function of particular experimental conditions.

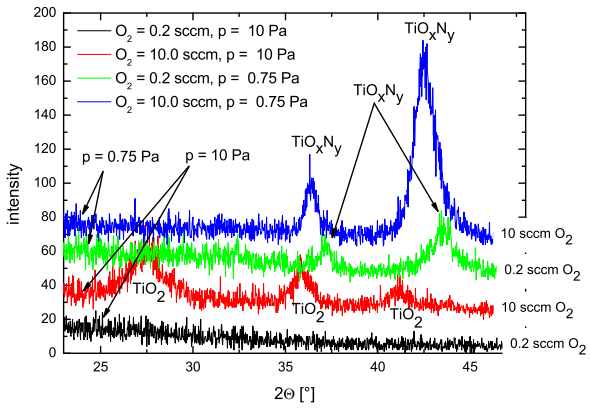

Fig. 6. The XRD patterns of deposited thin films at different experimental conditions. As a TiO_xN_y were identified x-ray peaks of films prepared at low flow rate of O_2. The TiO_xN_y peaks of XRD patterns for $p = 0.75$ Pa and 0.2 sccm (green line) are shifted towards lower angles because of lower oxygen/nitrogen contents in the film composition. At higher F_{O2} rutile or TiO_2 x-ray amorphous films are formed.

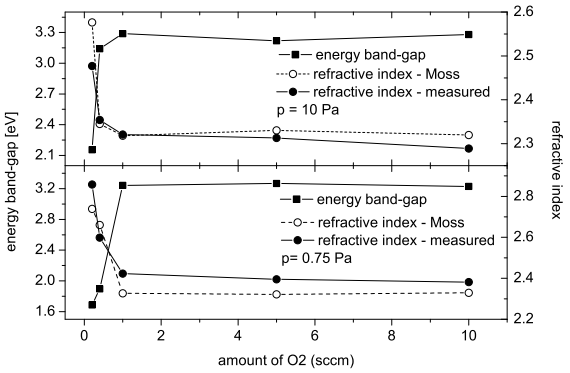

Fig. 7. Energy band-gap and refractive index as a function of the amount of O_2 in the discharge for different discharge pressure: $p = 10$ Pa (upper panel), $p = 0.75$ Pa (lower panel). The full circle symbols represents refractive index calculated from SE measurement at $\lambda = 500$ nm. The open circle symbols represents refractive index calculated from the Moss rule using values of the band-gap.

Thin films deposited at high oxygen flow rate ($F_{O2} \sim 10$ sccm) consist of TiO_2, which is found to be x-ray amorphous for high deposition pressure ($p \sim 10$ Pa) or forms rutile phases at low pressure ($p \sim 0.75$ Pa), respectively. The deposition of x-ray amorphous films at 10 Pa is probably due to lower energy transfer to the growing layer caused by increased number of particle collisions in plasma[42,43,46].

Fcc TiX (where X = O or N) is found at low oxygen flow. However, it is difficult to distinguish between TiO and TiN phases by x-ray diffractometry. Both structures show a cubic face centred Ti sublattice with oxygen or nitrogen incorporated in octahedral sites. Octahedral sites are filled completely if the ratio X/Ti = 1. This ratio can vary between 0 - 1 as a function of different deposition condition [65–68]. However, the lattice constant depends on the amount of octahedral sites filled by anions and, of course, also on the incorporated elements. Hence it is impossible to determine both type of elements and the amount of incorporated atoms only from the lattice constant measurement by XRD technique. Because both N and/or O are incorporated and we do not know the ratio of O/N Vegards law can not be used. Hence, for our films we assume incorporation of both oxygen and nitrogen into the Ti lattice. This assumption is confirmed by XPS measurements. Their composition is therefore referred as TiO_xN_y.

For the samples prepared at low pressure the peak positions of TiO_xN_y are shifted towards lower angles compared to layers deposited at higher pressure. This implies larger lattice constants, i.e. a higher amount of incorporated interstitial atoms. The attain lattice constants determined from peak position are 4.23 Å for $p = 0.75$ Pa and 4.15 Å for $p = 10$ Pa. Theoretical lattice constants values are $a_{TiN} = 4.242$ Å and $a_{TiO} = 4.185$ Å. However, all deposited crystalline phases show comparably small grain sizes. Thus we assume x-ray amorphous amounts of TiO/TiN or TiO_2 to be present within the films, too.

3.4. *Energy band-gap - spectroscopic ellipsometry*

Spectroscopic ellipsometry (SE) was employed to investigate the optical properties of deposited TiO_xN_y thin films, namely the energy band-gap E_g and refractive index n. If the flow rate of oxygen is decreased, E_g is decreased, too - see Fig. 7. Similar behaviour of energy band-gap was observed in [25] as well. The lowest values of $E_g \approx 1.7$-2.1 eV are related to TiO_xN_y structure with incorporated nitrogen into the Ti-O lattice as described above. The highest values of band-gap energy $E_g \approx 3.2$ eV were measured for highly oxidized gas mixtures with oxygen flow ≥ 1 sccm independent of the total pressure. This value corresponds with band gap of TiO_2 [69].

The band-gap is related to the refractive index by semi-empirical relation known as Moss rule [70,71]), $n^4 \cdot E_g = const.$, where $const. = 95$ eV. Comparison of refractive index values estimated from SE measurements for λ =500 nm and by Moss rule employing E_g is displayed in Fig. 7. Crystalline phase of TiO_xN_y shows higher values of refractive index n. A shift of maxima of $n(\lambda)$ distribution towards lower photon energies compared to TiO_2 prepared at high oxygen flow rate (not presented in the figure) was also observed.

The explanation of such behaviour was proposed in [25]. It is based on former research of Futsuhara et al. [72] who found that the band-gap is related to the difference in ionicity of metal-O and metal-N bonds. The electronegativity of oxygen is larger than that of nitrogen, which indicates that the Ti-O bonds involve a larger charge transfer than Ti-N bonds. Assuming that both, Ti-O as well as Ti-N, bonds coexist in the films, the shift of the band-gap to lower energy can be attributed to a decrease of ionicity due to formation of Ti-N bonds at lower oxygen flow rate.

4. Conclusion

The formation of TiO_xN_y by HiPIMS without post-deposition thermal annealing is proved in this report. The formation of TiO_xN_y is conditional to low partial pressure of nitrogen in (Ar)-N_2-O_2 reactive discharge atmosphere. If sufficient amount of oxygen is present in the discharge volume, x-ray amorphous TiO_2 (at higher pressure $p = 10$ Pa) or rutile phase of TiO_2 (at lower pressure $p = 0.75$ Pa) is formed. Local domains of TiN and/or TiO with fcc structure are formed at low flow of oxygen $F_{O2} < 0.5$ sccm. The Ti-N bonds that exist in TiO_xN_y structure are responsible for a decrease of the energy band-gap to the value $E_g \approx$ 1.7-2.1 eV and an increase of the refractive index n. The refractive index estimated from SE measurements corresponds very well to the values determined from semi-empirical Moss rule.

Acknowledgements

This work was supported by Deutsche Forschungsgemeinschaft through SFB/TR 24. Further projects KAN301370701, M100100915 of ASCR and research plan 1M06002 of Ministry of Education, Youth and Sports of the Czech Republic are acknowledged.

References

[1] A. Fujishima, K. Honda, Nature **238**, (1972), 37.
[2] E. Finazzi, C. Valentin, A. Selloni, G. Pacchioni, J. Phy. Chem. C **111**, (2007), 9275.
[3] S. Klosek, D. Raftery, J. Phys. Chem. B **105**, (2001), 2815.
[4] W. Choi, A. Termin, M.R. Hofmann, J. Phys. Chem. **98**, (1994), 13669.
[5] A.K. Ghos, H.P. Maruska, J. Electrochem. Soc. **124**, (1977), 1516.
[6] K. Zakrzewska, M. Radecka, A. Kruk, W. Osuch, Thin Solid Films **157**, (2003), 349.
[7] J.L. Gole, J.D. Stout, C. Burda, Y. Lou, X. Chen, J. Phys. Chem. B **108**, (2004), 1230.
[8] O. Diwald, T.L. Thomson, T. Zubkov, E.G. Goralski, S.D. Walck, J.T. Yates, J. Phys. Chem. B **108**, (2004), 6004.
[9] R. Asahi, T. Morikawa, T. Ohwaki, K. Aoki, Y. Taga, Science **293**, (2001), 269.
[10] T. Lindgren, J.M. Mwabora, E. Avendano et al, J. Phys. Chem. B **107**, (2003), 5709.
[11] C. Lettmann, K. Hildenbrand, H. Kish, W. Macyk, W.F. Maier, Appl. Catal. B **32**, (2001), 215.
[12] T. Umebayashi, T. Yamaki, H. Itoh, K. Asai, Appl. Phys. Lett. **81**, (2002), 454.
[13] J.C. Yu, J.G. Yu, W.K. Ho, Y.T. Jiang, L.Y. Yhang, Chem. Mater **14**, (2002), 3808.
[14] T. Morikawa, R. Asahi, T. Ohwaki, K. Aoki, Y. Taga, Jap. J. Appl. Phys. **40/6A**, (2001), L561.
[15] B. Farkas, J. Budai, I. Kabalci, P. Heszler, Zs. Geretovszky, Appl. Surf. Sci. **254**, (2008), 3484.
[16] L. Yhao, Q. Jiang, J. Lian, Appl. Surf. Sci.**254**, (2008), 4620.
[17] J. Park, J-Y. Lee, J.-H. Cho, J. Appl. Phys. **100**, (2006), 113534.
[18] M. Gartner, P. Osiceanu, M. Anastasescu et al, Thin Solid Films **516**, (2008), 8184.
[19] Ch. Trapalis, T. Giannakopoulou, N. Todorova et al, IEEE , (2007), 303.
[20] E. Martinez-Ferrero, Y. Sakatani, C. Boissiere et al, Adv. Funct. Matter **17**, (2007), 3348.
[21] P.G. Wu, C.H.Ma, J.K. Shang, Appl. Phys. **A81**, (2005), 1411.
[22] M.C. Yang, T.S. Yang, M.S. Wong, Thin Solid Films **469**, (2004), 1.
[23] S-W. Park, J-E. Heo, Sep. Purifi. Technol. **58**, (2007), 200.
[24] S-M. Chiu, Y-S Chen, K-Y. Yang, Y-L. Hsu, D. Gan, J. Mater. Precess. Technol. **192**, (2007), 60.
[25] S.H. Mohamed, O. Kapperty, J.M. Ngaruiya et al, Phys. Stat. Sol. A **201**, (2004), 90.
[26] S.H. Mohamed, O. Kapperty, T. Niemeier, R. Drese, M.M. Wakkad, M. Wuttig, Thin Solid Films **201**, (2004), 90.
[27] J.-M. Chappe, N. Martin, J.F. Pierson, et al, Appl. Surf. Sci. **225**, (2004), 29.
[28] Q. Li, J.K. Shang, J. Am. Ceram. Soc. **9**, (2008), 3167.
[29] N. Martin, J. Lintymer, J. Gavoille et al, Surf. Coat. Technol. **201**, (2007), 7720.
[30] J.-M. Chappe, N. Martin, J. Lintymer, et al, Appl. Surf. Sci. **253**, (2007), 5312.

[31] N. Martin, J. Lintymer, J. Gavoille et al, Surf. Coat. Technol. **201**, (2007), 7753.
[32] G. He, L.D. Yhang, G.H. Li, M. Liu, X.J. Wang, J. Phys. D: Appl. Phys. **41**, (2008), 045304.
[33] M. Balaceanu, V. Braic, M. Braic at al, Surf. Coat. Technol. **208**, (2008), 2384.
[34] D. Herman, J. Sicha, J. Musil, Vacuum **81**, (2006), 285.
[35] S. Schiller, K. Godicke, J. Reschke, V. Kirchhoff, S. Schneider, F. Milde, Surf. Coat. Technol. **61**, (1993), 331.
[36] J.W. Bradley, T. Welzel, J. Phys. D: Appl. Phys. **42**, (2009), 093001.
[37] V. Kouznetsov, K. Macak, J.M. Schneider, U. Helmersson, I. Petrov, Surf. Coat. Technol. **122**, (2006), 293.
[38] J.T. Gudmundsson, J. Alami, U. Helmersson, Appl. Phys. Lett. **78**, (2001), 3427.
[39] U. Helmersson, M. Lattermann, J. Blohmark, A.P Ehiasarian, J.T. Godmundsson, Thin Solid Films **513**, (2006), 1.
[40] J. Bohlmark, M. Lattermann, J. T. Gudmundsson at al, Thin Solid Films **300**, (1997), 1522.
[41] A. Vethuska, A.P. Ehiasarian, J. Phys. D: Appl. Phys. **41**, (2008), 015204.
[42] V. Stranak, M. Quaas, H. Wulff, Z. Hubicka, S. Wrehde, M. Tichy, R. Hippler, J. Phys. D: Appl. Phys. **41**, (2008), 055202.
[43] V. Stranak, M. Cada, M. Quaas et al., J. Phys. D: Appl. Phys. **42**, (2009), 105204.
[44] J. Alami, K. Sarakinos, F. Uslu, C. Klever, J. Dukwen, M. Wuttig, J. Phys. D: Appl. Phys. **42**, (2009), 115204.
[45] V. Stranak, Z. Hubicka, P. Adamek et al., Surf. Coat. Technol. **201**, (2006), 2512.
[46] J. Musil, D. Herman, J. Sicha, J. Vac. Sci. Technol. A. **24/3**, (2006), 521.
[47] Z. Navratil, D. Trunec, R. Smid, L. Lazar, Czech. J. Phys. **56/B**, (2006), B944.
[48] H. Wulff, H. Steffen, Characterisation of thin films; in: Low temperature plasma physics, R. Hippler, H. Kersten, M. Schmidt, K.-H. Schoenbach, Eds., Wiley-VCH, Berlin, (2008), 329.
[49] Powder Diffraction File, Joint Committee on Powder Diffraction - International Centre for Diffraction Data (NIST).
[50] E. D. Palik, Handbook of Optical Constants of Solids. Academic Press, (1985).
[51] H.G. Tomkins, Spectroscopic ellipsometry and Reflectometry. Wiley, New York, (1999).
[52] Z. Wang, S.A. Cohen, D.N. Ruzic, M.J. Goeckner, Phys. Rew. E **61/2**, (2000), 1904.
[53] K. Tao, D. Mao, J. Hopwood, J. Appl. Phys. **91**, (2002), 4040.
[54] A. Ricard, Reactive plasma. Sociate Francaise du Vide, Paris, (1996).
[55] B. Gordiets, A. Ricard, Plasma Sources Sci. Technol. **2**, (1993), 158.
[56] V. Kudrle, P. Vasina, A. Talsky, J. Janca, Czech. J. Phys. **52/D**, (2002), 589.
[57] A.V. Pipa, T. Bindemann, R. Foest, E. Kindel, J. Roepcke, K.-D. Weltmann, J. Phys. D: Appl. Phys. **41**, (2008), 194011.
[58] D. Depla, S. Heirwegh, S. Mahieu, R. De Gryse, J. Appl. Phys. **101**, (2007), 13301.
[59] J. Bohlmark, M. Lattermann, J.T. Gudmundsson et al., Thin Solid Films **515**, (2006), 1522.
[60] R. Ranjan, J.P. Allain, M.R. Hendricks, D.N. Ruzic, J. Vac. Sci. Technol. A**19/3**, (2001), 1004.
[61] M. Audronis, V. Bellido-Gonzales, Thin Solid Films **518**, (2010), 1962.
[62] M. Audronis, V. Bellido-Gonzales, B. Daniel, Surf. Coat. Technol. **607**, (2010), XX.in print
[63] E. Wallin, U. Helmersson, Thin Solid Films **516**, (2008), 6398.
[64] N. Martin, D. Baretti, C. Rousselot, J.-Y. Rauch, Surf. Coat. Technol. **107**, (1998), 172.
[65] B. Holmberg, Acta Chemica Scandinavica **16**, (1962), 1255.
[66] J. Chorn-Cherng, T. Goto, T. Hirai, J. Alloys Compd. **190**, (1993), 197.
[67] E. Etchessahar, J.P. Bars, J. Debuigne, J. Less-Common Metals **134**, (1987), 123.
[68] H. Kersten, H.-E. Wagner and H. Wulff, C. Eggs, Thin Solid Films **290-291**, (1996), 381.
[69] A. Fujishima, X. Zhang, D.A. Tryk, Surf. Sci. Rep. **63**, (2008), 515.
[70] T.S. Moss, Proc. Phys. Soc. B **63**, (1950), 167.
[71] R.R. Reddy, Y. Nazeer Ahammed, Infrared. Phys. Technol. **36**, (1995), 825.
[72] M. Futsuhara, K. Yoshioka, O. Takai, Thin Solid Films **171**, (1998), 322.